Inorganic Chemistry

Article

pubs.acs.org/IC

Anions Influence the Relaxation Dynamics of Mono-μ_3-OH-Capped Triangular Dysprosium Aggregates

Li Zhang,[†,‡] Peng Zhang,[†,‡] Lang Zhao,[†] Jianfeng Wu,[†,‡] Mei Guo,[†,‡] and Jinkui Tang*[,†]

[†]State Key Laboratory of Rare Earth Resource Utilization, Changchun Institute of Applied Chemistry, Chinese Academy of Sciences, Changchun 130022, P. R. China

[‡]University of Chinese Academy of Sciences, Beijing 100049, P. R. China

Supporting Information

ABSTRACT: A family of four Dy_3 triangular circular helicates, namely, $[Dy_3(HL)_3(\mu_3\text{-}OH)(CH_3OH)_2(H_2O)_4]Cl_{1.5}(OH)_{0.5}\cdot 0.5H_2O$ (**1**), $[Dy_3(HL)_3(\mu_3\text{-}OH)(CH_3OH)_3(H_2O)_2Cl]Cl\cdot CH_3OH$ (**2**), $[Dy_3(HL)_3(\mu_3\text{-}OH)(CH_3OH)_3(H_2O)_2(NO_3)](NO_3)$ (**3**), and $[Dy_3(HL)_3(\mu_3\text{-}OH)(CH_3OH)_4(ClO_4)](ClO_4)$ (**4**), were assembled by the reaction of a new acylhydrazone ligand H_3L [(3-hydroxy)-*N*′-((8-hydroxyquinolin-2-yl)methylene)picolinohydrazide] with different dysprosium(III) salts. These compounds represent the first examples of $\mu\text{-}O_{acylhydrazone}$-bridged triangular Dy_3 SMMs reported to date. Alternating-current magnetic susceptibility measurements revealed that compounds **1** and **2** show typical SMM behavior with the occurrence of multiple relaxation processes, whereas frequency-dependent relaxation signals without χ'' peaks were observed in **3** and **4** under zero dc field. Such distinct dynamic behaviors are attributed to the different sizes of the terminal coordination solvent/anions (H_2O, Cl^-, NO_3^-, and ClO_4^- for **1**−**4**, respectively) at the Dy_3 site. Here, similar deviations from the ideal monocapped square-antiprismatic (C_{4v}) geometry defined by SHAPE software were observed around local Dy centers in **1** and **2**, whereas the situation was completely different in **3** and **4** as a result of the presence of relatively large anions in the limited space defined by three intercrossing rigid hydrazone ligands.

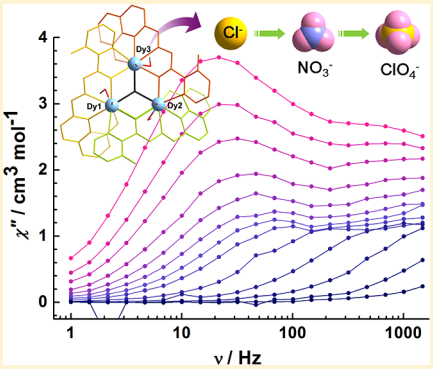

INTRODUCTION

Single-molecule magnets (SMMs) with the slow relaxation of magnetization deriving from molecular-based blocking anisotropy have been a burgeoning topic of intense interest to physical, chemical, and materials scientists over the past two decades because of their exotic technological applications in high-density information storage, quantum computing, and spintronics.[1−9] Since the seminal discovery that Ishikawa et al.'s double-decker compound $(Bu_4N)[Tb(Pc)_2]$ (H_2Pc = phthalocyanine) shows slow relaxation of the magnetization at low temperatures,[10] considerable attention has been directed toward introducing 4f ions in to elaborate high-barrier SMMs in either mixed 3d/4f or pure 4f systems as a result of their inherent magnetic anisotropy arising from a large, unquenched orbital angular momentum.[11,12] Certainly, dysprosium plays a crucial role in the exploitation of lanthanide-based SMMs because of its unparalleled single-ion anisotropy and the spin-parity effect for a Kramers ion (odd number of 4f electrons) and is thus responsible for numerous ground-breaking results,[13−19] such as the record anisotropic energy barriers of U_{eff} = 692 K in the $\{Dy_4K_2\}$ system.

The meteoric progress in this field makes clear that the alteration of the coordination environment on local metal centers is of great importance in modulating the relaxation dynamics of lanthanide-based SMMs.[20−26] For instance, the group of Tong[24] synthesized a [Zn−Dy−Zn] single-ion magnet (SIM), where the switching of the anisotropy barrier was realized by a change in the coordination geometry around the Dy^{III} site from pentagonal-bipyramidal (quasi-D_{5h}) to octahedral (quasi-O_h) through a single-crystal-to-single-crystal (SCSC) transformation, an important approach to probing the importance of the local symmetry on the performance of SIMs. In addition, the replacement of auxiliary ligands in some β-diketone-based mononuclear dysprosium compounds has also been shown to play a crucial role in controlling the local coordination geometries of the Dy^{III} ions associated with the relaxation process.[23,27] More importantly, Sessoli and co-workers revealed that even a change in hydrogen bonding in the coordinated water molecule has a significant impact on the orientation of the anisotropy axis in a Dy/DOTA compound (DOTA = tetraazacyclododecane tetraacetic acid).[28]

Herein, with the aim of investigating the influence of anion size on the local coordination geometry and eventually the relaxation behavior in Dy^{III} compounds, we employed $DyCl_3$, $Dy(NO_3)_3$, and $Dy(ClO_4)_3$ salts as the origins of anions of different sizes and assembled them with the new aroylhydrazone ligand (3-hydroxy)-*N*′-((8-hydroxyquinolin-2-yl)-methylene)picolinohydrazide (H_3L). As a result, a family of four Dy_3 triangular circular helicates, namely, $[Dy_3(HL)_3(\mu_3\text{-}$

Received: March 27, 2015
Published: May 18, 2015

DOI: 10.1021/acs.inorgchem.5b00702
Inorg. Chem. 2015, 54, 5571−5578

Table 1. Crystallographic Data and Structure Refinement Details of Compounds 1−4

	compound			
	1	2	3	4
formula	$(C_{50}H_{48.5}Cl_{1.5}Dy_3N_{12}O_{17})_2$	$C_{52}H_{51}Cl_2Dy_3N_{12}O_{16}$	$C_{51}H_{47}Dy_3N_{14}O_{21}$	$C_{52}H_{47}Cl_2Dy_3N_{12}O_{22}$
Mr	3260.37	1658.45	1679.53	1750.42
crystal system	orthorhombic	monoclinic	triclinic	triclinic
space group	*Ibam*	$P2_1/c$	$P\bar{1}$	$P\bar{1}$
T (K)	296(2)	296(2)	296(2)	296(2)
a (Å)	26.881(3)	12.1432(6)	12.0267(7)	12.2026(5)
b (Å)	28.411(3)	13.8045(7)	14.5603(8)	14.7513(6)
c (Å)	36.617(4)	34.8017(18)	16.7639(10)	17.1605(7)
α (deg)	90	90	82.9470(10)	77.9870(10)
β (deg)	90	91.5890(10)	88.0140(10)	86.5850(10)
γ (deg)	90	90	80.4420(10)	78.2860(10)
V (Å^3)	27965(6)	5831.6(5)	2872.6(3)	2957.9(2)
Z	8	4	2	2
ρ_{calcd} (g cm^{-3})	1.549	1.888	1.942	1.965
μ(Mo Kα) (mm^{-1})	3.296	3.974	3.953	3.931
F (000)	12672	3224	1634	1702
reflns collected	83746	36315	18210	18814
unique reflns	14049	11562	11327	11683
R_{int}	0.1078	0.0447	0.0438	0.0323
parameters/restraints	765/18	774/12	808/0	827/0
GOF	1.051	1.025	1.009	1.035
R_1 [$I > 2\sigma(I)$]	0.0680	0.0361	0.0512	0.0442
wR_2 (all data)	0.2567	0.0827	0.1394	0.1253

$OH)(CH_3OH)_2(H_2O)_4]Cl_{1.5}(OH)_{0.5}\cdot 0.5H_2O$ (**1**), $[Dy_3(HL)_3(\mu_3\text{-}OH)(CH_3OH)_3(H_2O)_2Cl]Cl\cdot CH_3OH$ (**2**), $[Dy_3(HL)_3(\mu_3\text{-}OH)(CH_3OH)_3(H_2O)_2\ (NO_3)](NO_3)$ (**3**), and $[Dy_3(HL)_3(\mu_3\text{-}OH)(CH_3OH)_4(ClO_4)](ClO_4)$ (**4**), were isolated, and their magnetic properties were characterized in detail. Direct-current (dc) magnetic susceptibility measurements of compounds **1**−**4** indicated similar static magnetic behaviors. Alternating-current magnetic susceptibility measurements revealed that **1** and **2** exhibit multiple relaxation processes, whereas **3** and **4** exhibit merely frequency-dependent slow magnetic relaxation under zero dc field.

EXPERIMENTAL SECTION

Materials and Measurements. All reagents and solvents were of A.R. grade and were used without further purification. Elemental analysis (C, H, and N) was performed with a Perkin-Elmer 2400 analyzer. Fourier transform infrared (FTIR) spectra (Figure S1, Supporting Information) were recorded with a Perkin-Elmer Fourier transform infrared spectrophotometer using the reflectance technique (4000−300 cm^{-1}). Samples were prepared as KBr disks. Magnetic susceptibility measurements were carried out on a Quantum Design MPMS-XL7 superconducting quantum interference device (SQUID) magnetometer equipped with a 7 T magnet. Direct-current (dc) measurements were collected with an external magnetic field of 1000 Oe in the temperature range of 1.9−300 K, and alternating-current (ac) measurements were carried out in a 3.0 Oe ac field oscillating at different frequencies from 1 to 1500 Hz. The experimental magnetic susceptibility data were corrected for the diamagnetism estimated from Pascal's tables[29] and sample-holder calibration.

Synthesis of the Ligand. 3-Hydroxypicolinohydrazide was prepared by the literature procedure previously reported.[30] The Schiff-base ligand H_3L [(3-hydroxy)-*N*′-((8-hydroxyquinolin-2-yl)-methylene)picolinohydrazide] was synthesized by a simple hydrazone condensation reaction of 3-hydroxypicolinohydrazide (10 mmol, 1.53 g) and 8-hydroxyquinoline-2-carbaldehyde (10 mmol, 1.73 g) in a 1:1 ratio in methanol (50 mL). Then, the reaction mixture was stirred overnight at room temperature. The yellow precipitate formed was filtered off and washed with methanol. Yield: 90%. ^{1}H NMR ($CDCl_3$, δ, ppm): 12.12 (s, 1H, −O*H*), 9.51 (s, 1H, −N*H*), 8.47 (d, 1H, −C*H*), 7.25−7.65 (8H, Ar−*H*), 7.81 (s, 1H, −O*H*). IR (KBr, cm^{-1}): 3384 (w), 3276 (m), 3056 (br), 1676 (s), 1538 (s), 1508 (s), 1467 (s), 1446 (s), 1326 (s), 1296 (s), 1238 (s), 1183 (s), 1146 (m), 1118 (s), 949 (w), 839 (m), 802 (m), 751 (m), 721 (m), 668 (m).

Synthesis of $[Dy_3(HL)_3(\mu_3\text{-}OH)(CH_3OH)_2(H_2O)_4]Cl_{1.5}(OH)_{0.5}\cdot 0.5H_2O$ (1). $DyCl_3\cdot 6H_2O$ (0.1 mmol, 0.038 g) was added to a suspension of H_3L (0.1 mmol, 0.031 g) in CH_3OH/CH_3CN (10 mL/5 mL), and then Et_3N (0.2 mmol, 0.028 mL) was added. The resultant red solution was stirred for 4 h and subsequently filtered. The filtrate was exposed to air to allow the slow evaporation of the solvent. Dark red needles of **1** suitable for X-ray diffraction analysis were collected after 2 weeks. Yield: 20 mg (37%, based on Dy). Elemental analysis (%): calcd for $C_{50}H_{48.50}Cl_{1.50}Dy_3N_{12}O_{17}$ C, 36.84, H, 3.00, N, 10.31; found C, 36.59, H, 2.97, N, 10.12. IR (KBr, cm^{-1}): 3321 (br), 3216 (br), 1636 (w), 1588 (s), 1547 (w), 1521 (s), 1496 (s), 1477 (s), 1443 (s), 1377 (m), 1331 (s), 1306 (s), 1279 (m), 1249 (m), 1214 (s), 1103 (m), 1074 (m), 1048 (m), 971 (w), 928 (w), 905 (w), 832 (w), 767 (w), 767 (w), 707 (w), 677 (w), 567 (w), 533 (w).

Synthesis of $[Dy_3(HL)_3(\mu_3\text{-}OH)(CH_3OH)_3(H_2O)_2Cl](Cl)\cdot CH_3OH$ (2). Diethyl ether was allowed to diffuse slowly into the filtrate obtained from **1** at room temperature, and red plates of **2** formed in 1 week. Yield: 16 mg (29%, based on Dy). Elemental analysis (%): calcd for $C_{52}H_{51}Cl_2Dy_3N_{12}O_{16}$ C, 37.66, H, 3.10, N, 10.13; found C, 37.29, H, 3.09, N, 10.25. IR (KBr, cm^{-1}): 3216 (br), 1651 (w), 1585 (s), 1546 (w), 1522 (s), 1495 (s), 1476 (s), 1444 (s), 1376 (m), 1331 (s), 1304 (m), 1276 (m), 1247 (m), 1214 (s), 1105 (m), 1072 (w), 1047 (w), 1030 (w), 971 (w), 930 (w), 904 (w), 838 (w), 815 (w), 767 (w), 737 (w), 676 (w), 567 (w), 535 (w).

Synthesis of $[Dy_3(HL)_3(\mu_3\text{-}OH)(CH_3OH)_3(H_2O)_2(NO_3)](NO_3)$ (3). $Dy(NO_3)_3\cdot 6H_2O$ (0.1 mmol, 0.046 g) was added to a suspension of H_3L (0.1 mmol, 0.031 g) in CH_3OH/CH_2Cl_2 (10 mL/10 mL), and then Et_3N (0.3 mmol, 0.042 mL) was added. The resultant red solution was stirred for 4 h and subsequently filtered. The filtrate was exposed to air to allow the slow evaporation of the solvent. Red needles of **3** suitable for X-ray diffraction analysis were collected after 1 week. Yield: 28 mg (50%, based on Dy). Elemental analysis (%): calcd for $C_{51}H_{47}Dy_3N_{14}O_{21}$ C, 36.47, H, 2.82, N, 11.68; found C, 36.50, H,

DOI: 10.1021/acs.inorgchem.5b00702
Inorg. Chem. 2015, 54, 5571−5578

2.79, N, 11.72. IR (KBr, cm^{-1}): 3591 (w), 3354 (br), 3069 (br), 2810 (br), 1588 (s), 1546 (w),1523 (s), 1495 (m), 1474 (m), 1445 (s), 1376 (m), 1330 (s), 1302 (s), 1250 (m), 1216 (m), 1104 (m), 1075 (w), 1017 (w), 930 (w), 905 (w), 838 (w), 806 (w), 760 (w), 707 (w), 677 (w), 569 (w).

Synthesis of $[Dy_3(HL)_3(\mu_3\text{-}OH)(CH_3OH)_4(ClO_4)](ClO_4)$ (4). A procedure similar to that used for **3** but with $Dy(ClO_4)_3{\cdot}6H_2O$ (0.1 mmol, 0.057 g) and Et_3N (0.2 mmol, 0.028 mL) afforded compound **4**. Dark red blocks of **4** suitable for X-ray diffraction analysis were collected after 10 days. Yield: 22 mg (38%, based on Dy). Elemental analysis (%): calcd for $C_{52}H_{47}Cl_2Dy_3N_{12}O_{22}$ C, 35.68, H, 2.71, N, 9.60; found C, 36.03, H, 2.66, N, 9.69. IR (KBr, cm^{-1}): 3430 (br), 3077 (br), 2817 (br), 1633 (w), 1588 (s), 1545 (w), 1521 (s), 1494 (s), 1473 (s), 1443 (s), 1376 (m), 1328 (s), 1305 (s), 1276 (w), 1248 (m), 1217 (m), 1103 (s), 1058 (s), 969 (w), 930 (w), 906 (w), 841 (w), 804 (w), 757 (w), 738 (w), 694 (w), 621 (w), 569 (w), 535 (w).

X-ray Crystallography. Crystallographic data for **1**–**4** were collected on a Bruker Apex II charge-coupled device (CCD) diffractometer with graphite-monochromated Mo Kα radiation (λ = 0.71073 A°) at 296(2) K. The structure was solved by direct methods and refined on F^2 by full-matrix least-squares using SHELXS-97 and SHELXL-97.[31] The locations of Dy atoms were easily determined, and O, N, C and Cl atoms were subsequently determined from the difference Fourier maps. All non-hydrogen atoms were refined with anisotropic thermal parameters. The H atoms were introduced in calculated positions and refined with a fixed geometry with respect to their carrier atoms. Details for the crystallographic data and refinement are summarized in Table 1, and selected bond distances and angles are listed in Table S1 (Supporting Information).

RESULTS AND DISCUSSION

For the monohydrazone ligand H_2L' (Scheme 1), the presence of two such linearly arranged coordination pockets (A and B)

Scheme 1. Relationship between the Feature of Coordination Pockets and the Resultant Products[a,b]

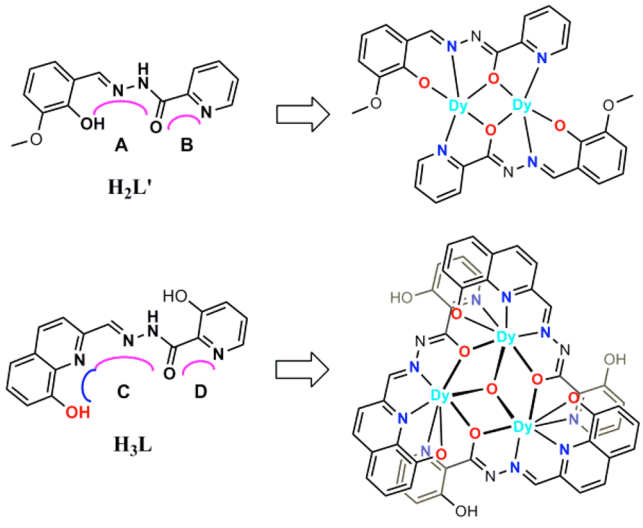

[a]Coordinated solvent molecules and anions omitted for clarity. [b]A–D represent coordination pockets.

sharing a carbonyl oxygen atom is generally known to result in a propensity for the formation of centrosymmetric or asymmetric Dy_2 compounds,[20,32–34] in which two ligands are coordinated to dysprosium centers in an antiparallel or parallel fashion (Scheme 1, top). The feature of coordination pockets in a linear arrangement almost rules out the possibility of assembling dysprosium triangles or other polynuclear clusters with odd numbers of Ln ions, as supported by numerous recent examples employing this type of monohydrazone ligand and their analogues such as H_2L'.[20,35,36] With this in mind, an additional coordinated site (phenol groups) of the aldehyde part of the ligand was introduced to alter the angle of pocket A, which promotes the potential for nonparallel arrangement of ligands. As expected, μ_3-hydroxo-bridged triangular circular helicates were successfully synthesized, with three dideprotonated HL^{2-} ligands around the central Dy_3O in a head-to-tail fashion at an angle of about 60° (Scheme 1, bottom). It is worth mentioning that this is the first observation of such μ-$O_{acylhydrazone}$-bridged Dy_3 trianglar SMMs.

Structure Descriptions. The reactions of ligand H_3L with the corresponding dysprosium salts under basic conditions yielded compounds **1**–**4**, whose molecular structures are depicted in Figure 1. Single-crystal X-ray diffraction studies revealed that compounds **1**–**4** are essentially isomorphous, sharing a similar triangular core structure, and that they mainly differ in the terminal ligands (solvent or anion) around the Dy3 ions.

Remarkably, such a Dy_3 triangle is capped by only one μ_3-hydroxo bridge, lying approximately 0.6825, 0.6582, 0.6757, and 0.7135 Å above the Dy_3 plane for compounds **1**–**4**, respectively, which appears to be distinct from the results for previously reported Dy_3-related compounds.[2,15,37–40] Some important bond distances and angles for the central $[Dy_3O_4]$ cores of **1**–**4** are compared in Table S1 (Supporting Information). For **1**–**4**, three almost-equal edges (Dy···Dy distances) of the triangle and Dy···Dy···Dy angles close to 60° reveal a nearly equilateral Dy_3 triangle. The resultant $[Dy_3(\mu_3\text{-}OH)]^{8+}$ core is surrounded by three intercrossing rigid HL^{2-} ligands along a pseudo-3-fold axis defined by Dy1, Dy2, and Dy3, thus resulting in a limited space within a triangular circular helicate (Figure 2). Herein, each HL^{2-} ligand bridges two Dy^{III} ions through one carbonyl oxygen atom (O2, O5, and O8), adopting the deprotonated enol form in a $2.1_12_{12}01_11_101_2$ binding mode (Scheme S1, Supporting Information) indicated by Harris notation.[41] This notation describes the coordination mode as $[X.Y_1Y_2Y_3\cdots Y_n]$, where X is the overall number of metal atoms bound by the whole ligand and each value of Y refers to the number of metals attached to the different donor atoms.

A critical difference for compounds **1**–**4** is the distinct terminal coordination anions at the Dy3 site, namely, H_2O, Cl^-, NO_3^- and ClO_4^-, respectively, which exhibit increasing size and, thus, have a prominent effect on the coordination environments around the Dy ions. As shown in Figure S2 (Supporting Information), the coordination environments of Dy1 and Dy2 in **1**–**3** are all completed by two solvent molecules (H_2O and CH_3OH) and adopt similar N_3O_6 spheres. It is noted that the Dy3 centers of **1**–**4** are nine-coordinated and, in addition to the coordination of the hydrazone ligands, the remaining sites are filled by one solvent molecule and H_2O, Cl^-, NO_3^-, and ClO_4^-, respectively. Remarkably, for **4**, the presence of the bulky ClO_4^- anion leads to the removal of one coordinated solvent molecule around Dy2 due to steric hindrance (Figure 2, right) and the distortion of the central core $[Dy_3O_4]$, with the increase of bond distance Dy1–O5 and the decrease of Dy2–O5 (Table S1, Supporting Information). Thus, Dy2 is eight-coordinated in **4**, and the three dysprosium centers are located in entirely distinct environments from those in compounds **1** and **2**.

The difference in local environments with respect to nine-coordinated Dy^{III} ions for compounds **1**–**4** was quantified by the continuous shape measures (CShM) approach using

DOI: 10.1021/acs.inorgchem.5b00702
Inorg. Chem. 2015, 54, 5571–5578

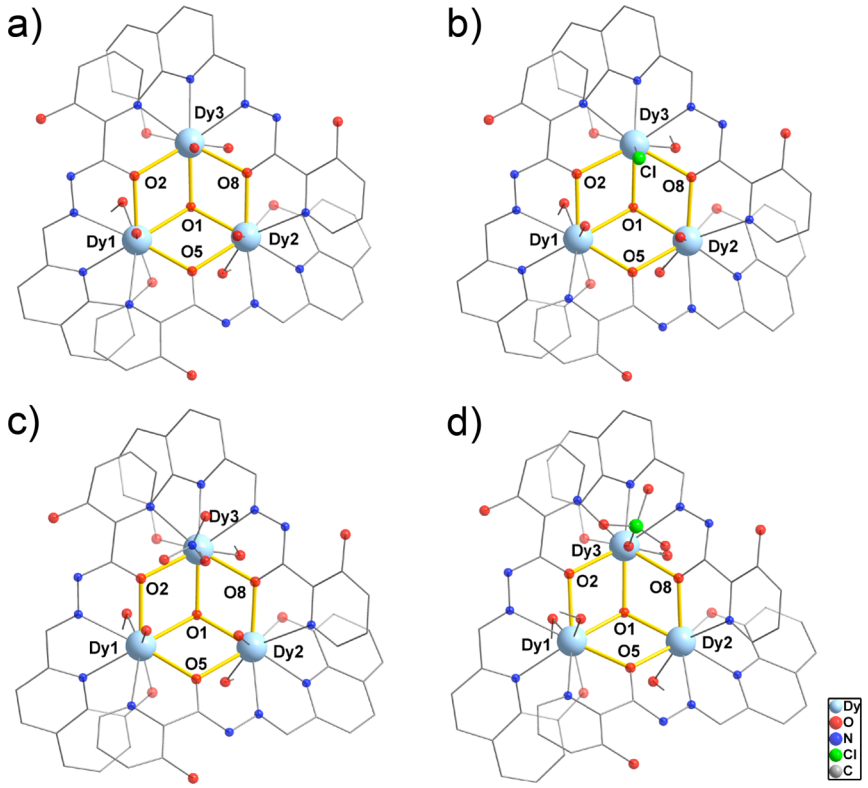

Figure 1. Partially labeled Dy_3 structures of compounds (a) **1**, (b) **2**, (c) **3**, and (d) **4**, with hydrogen atoms, solvent molecules, and external counteranions omitted for clarity.

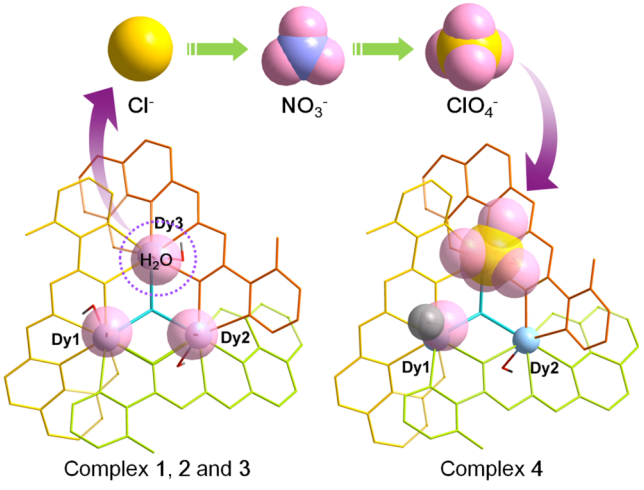

Figure 2. Crystal structures of (left) **1**−**3** and (right) **4** with the terminal ligand around Dy centers represented by space-filling models. The ligands are depicted in different colors to show the helicity. Color code: pale blue, Dy; pink, O; gold, Cl.

SHAPE software, which essentially allows one to evaluate numerically the extent of distortion from an ideal shape for a given structure (with zero being ideal).[42] As shown in Table 2, CShM analysis revealed that each Dy^{III} center in **1**−**4**, except for Dy2 in **4**, is best described as exhibiting a nine-coordinated monocapped square-antiprismatic (C_{4v}) geometry, but with greatly different distortions from the ideal geometry for all of the Dy^{III} ions. Compounds **1** and **2** exhibit close CShM values in the three corresponding Dy sites, indicating similar coordination environments in the two compounds, although the Dy−Cl bond distance in **2** [2.781(14) Å] is much longer than the Dy−O_{water} bond distance in **1** [2.386(10) Å]. In contrast, a significant change in CShM values around the Dy3 ion, indicating differences from compounds **1** and **2**, was observed in **3** and **4**, which should be the main result of the relatively large NO_3^- and ClO_4^- anions coordinated to Dy3 (Figure 2). Furthermore, this increasing steric hindrance at the Dy3 site also has an impact on the coordination geometries at the other two sites, as demonstrated in Table 2, and especially in **4**, the obvious effect results in completely different coordination environments at all three Dy sites from those in compounds **1** and **2**. As a result, distinct relaxation dynamics of magnetization were observed for compounds **1**−**4**, as discussed in the next section.

Table 2. Results of Continuous Shape Measures Analysis and Coordination Environment for the Nine-Coordinated Dy^{III} Ions in 1−4[a]

	Dy1	Dy2	Dy3
1	1.665 (O_6N_3)	1.310 (O_6N_3)	1.888 (O_6N_3)
2	1.709 (O_6N_3)	1.449 (O_6N_3)	1.872 (O_5N_3Cl)
3	1.768 (O_6N_3)	1.533 (O_6N_3)	1.486 (O_6N_3)
4	1.599 (O_6N_3)	− (O_5N_3)	1.270 (O_6N_3)

[a]Monocapped square antiprism (C_{4v}).

The packing arrangements in compounds **1**−**4** along the *a*, *b*, and *c* axes are presented in Figures S3 and S4 in the Supporting Information. Among the compounds, the packing arrangements in **3** and **4** are similar along different directions. Interestingly, the projection along the crystallographic *c* axis of **1** obviously shows two types of channels.

Magnetic Properties. Variable-temperature dc magnetic susceptibility data on polycrystalline samples revealed room-temperature $\chi_M T$ values of 41.0, 41.0, 39.7, and 40.9 cm^3 K

DOI: 10.1021/acs.inorgchem.5b00702
Inorg. Chem. 2015, 54, 5571−5578

mol^{-1} for **1**−**4**, respectively, which are relatively consistent with the theoretical value of 42.5 cm^3 K mol^{-1} expected for three uncoupled Dy^{III} ions ($S = {}^5/_2$, $L = 5$, $^6H_{15/2}$, $g = {}^4/_3$). The temperature dependences of the product $\chi_M T$, as shown in Figure 3 for all four of the compounds, display similar thermal

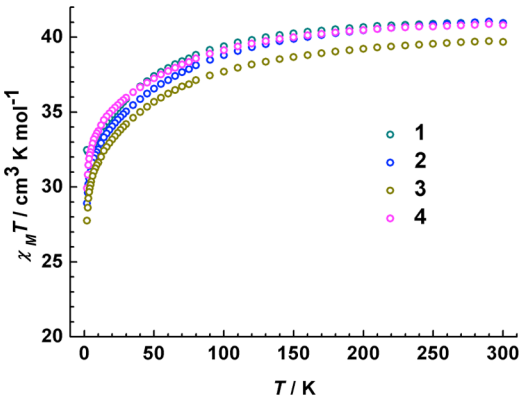

Figure 3. Temperature dependence of χT for **1**−**4**.

evolutions in the temperature range of 300−10 K, namely, a slight decline upon cooling, which possibly results from the thermal depopulation of excited Stark sublevels or large magnetic anisotropy in the Dy^{III} system. Below 10 K, $\chi_M T$ rapidly drops to a minimum value of 32.5, 28.9, 27.7, and 29.9 cm^3 K mol^{-1} for **1**−**4**, respectively, at 1.9 K, as a possible result of the different intramolecular antiferromagnetic interactions between the Dy centers in compounds **1**−**4**.

The field dependence of magnetization (M) for compounds **1**−**4** was also measured in the 0−70 kOe field range below 5 K (Figure S5, Supporting Information). Herein, the M versus H/T data were far from saturation, and the corresponding magnetization data did not lie on a single master curve at higher field below 5 K, which is indicative of the presence of significant magnetic anisotropy and/or low-lying excited states in all systems.[43]

The dynamic magnetic properties of **1**−**4** were investigated under zero/nonzero applied dc fields by using ac measurements under a 3 Oe field. As shown in Figure 4 (left) and Figure S6 (left) (Supporting Information), an obvious frequency- and temperature-dependent ac signal was observable under zero dc field for **1**, which is characteristic of SMM behavior. Furthermore, the $\chi''(\nu)$ plot clearly displays two peaks between 1.9 and 4.0 K, demonstrating the occurrence of two relaxation processes.[9] Therefore, two series of relaxation times (τ) could be extracted between 1.9 and 8.0 K by fitting the $\chi''(\nu)$ plots with the sum of two modified Debye functions[44]

$$\chi_{AC}(\omega) = \chi_{s,tot} + \frac{\Delta\chi_1}{1 + (i\omega\tau_1)^{(1-\alpha_1)}} + \frac{\Delta\chi_2}{1 + (i\omega\tau_2)^{(1-\alpha_2)}} \quad (1)$$

Arrhenius analysis [$\tau = \tau_0 \exp(U_{eff}/k_B T)$] for plots of ln τ versus T^{-1} afforded effective energy barriers (U_{eff}) of 45.9 and 7.6 K with pre-exponential factors (τ_0) of 3.15×10^{-7} and 2.27×10^{-5} s for the slow relaxation (SR) phase and fast relaxation (FR) phase, respectively, in the high-temperature (HT) range (Figure 5). In addition, the linear fitting in the low-temperature (LT) range further gave U_{eff} values of 3.2 and 1.6 K with corresponding τ_0 values of 1.88×10^{-3} and 6.97×10^{-5} s for the SR and FR, respectively. As a result, such a complicated

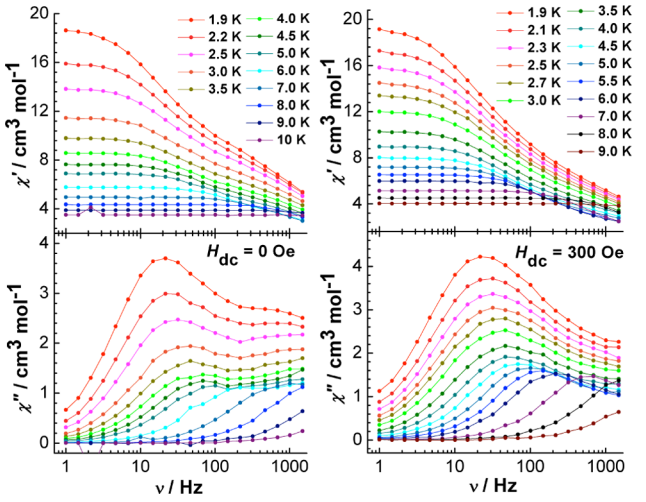

Figure 4. Frequency-dependent (top) in-phase and (bottom) out-of phase components of ac susceptibility data for **1** at the indicated temperature ranges under (left) a zero dc field and (right) an applied dc field of 300 Oe.

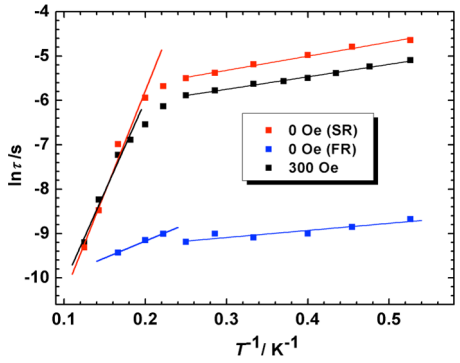

Figure 5. Magnetization relaxation time, ln τ, versus T^{-1}, for **1** under 0 and 300 Oe dc fields. The solid lines correspond to the best fits of the experimental data to the Arrhenius law.

relaxation process should be ascribed to the presence of different magnetic centers in this Dy_3 system.

The Cole−Cole diagrams (Figure S7, Supporting Information) exhibit two well-separated relaxation phases in the range of 1.9−6 K. However, as the temperature was increased, the FR gradually moved beyond the high-frequency limit (1500 Hz) of the magnetometer used, and only an asymmetric semicircle corresponding to SR at 7.0 and 8.0 K was observed. Fitting the data by eq 1 afforded α values in the ranges of 0.31−0.50 and 0.08−0.14 for FR and SR, respectively, implying a relatively wide distribution of the relaxation times for the FR process.

To further probe the dynamic magnetic behavior, the frequency dependence of the out-of-phase ac susceptibility (χ'') at various applied dc fields was collected for **1** at 1.9 K. As depicted in Figure S8 (Supporting Information), the ac peaks gradually moved to higher frequency as the field was increased, and the application of a dc field of 300 Oe induced the elimination of the high-frequency peaks, so that only a set of frequency-dependent peaks were observed in the range of 1.9−7.0 K (Figure 4, right). Meanwhile, the out-of-phase ac susceptibility (χ'') exhibited a slightly increasing tendency in the high-frequency range (>1000 Hz) within the frequency window, signaling the occurrence of an additional faster relaxation pathway, also seen from the Cole−Cole plots with

DOI: 10.1021/acs.inorgchem.5b00702
Inorg. Chem. 2015, 54, 5571−5578

Table 3. Characteristic Dynamic Parameters for 1 and 2

	H_{dc} (Oe)	$U_{(HT)}$ (K)	$\tau_{0(HT)}$ (s)	$U_{(LT)}$ (K)	$\tau_{0(LT)}$ (s)	α
1	0 (SR)	45.9	3.15×10^{-7}	3.2	1.88×10^{-3}	0.08−0.14
	0 (FR)	7.6	2.27×10^{-5}	1.6	6.97×10^{-5}	0.31−0.50
	300	41.2	6.61×10^{-7}	2.8	1.37×10^{-3}	0.03−0.31
2	1000	34.3	3.23×10^{-6}	–	–	0.21−0.48

the clear distortion of the asymmetrical semicircles below 6.0 K (Figure S9, Supporting Information). A linear fit of the experimental data to the Arrhenius law yielded the energy barriers of 41.2 and 2.8 K with pre-exponential factors of 6.61×10^{-7} and 1.37×10^{-3} s for the high- and low-temperature domains, respectively. Such values of energy barriers and relaxation times were found to be comparable to those for the SR process under zero dc field (Table 3).

Compared to compound **1**, compound **2** displays similar dynamic magnetic behavior with broad frequency-dependent peaks under zero dc field (Figure 6, left), suggesting the

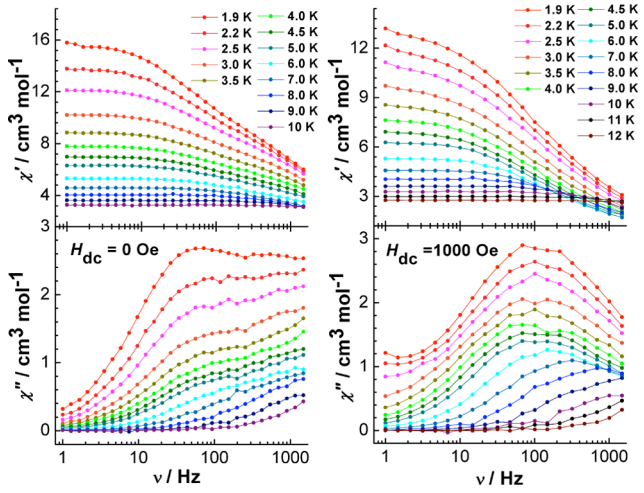

Figure 6. Frequency-dependent (top) in-phase and (bottom) out-of phase components of ac susceptibility for **2** at the indicated temperature ranges under (left) a zero dc field and (right) an applied dc field of 1000 Oe.

presence of more than one relaxation process, as a result of the similar coordination environments in the two compounds. The $\chi''(T)$ plot (Figure S10, left, Supporting Information) shows an unobvious broad shoulder between 2 and 12 K in the range of 120−1488 Hz. Unfortunately, in this case, the relaxation time (τ) cannot be obtained by fitting $\chi''(\nu)$ plots with the sum of two modified Debye functions, because of the absence of two perfectly well-separated peaks in the whole temperature range. However, application of a 1000 Oe dc field led to a series of well-resolved frequency-dependent peaks with an imaginary component in the 1.9−8.0 K range (Figure 6, right) from which the relaxation times could be extracted. In the high-temperature regime (>5.0 K), the relaxation obeys a thermally activated mechanism with U_{eff} = 34.3 K ($\tau_0 = 3.23 \times 10^{-6}$) based on the Arrhenius law, which is comparable to the barrier for compound **1** (Table 3). Below 5.0 K, the relaxation times (τ) deviate markedly from linearity and become temperature-independent, characteristic of quantum tunneling of magnetization (QTM). Therefore, the fit of the ln τ versus T^{-1} plot (Figure 7) to the equation

$$\tau^{-1} = \tau_{QT}^{-1} + \tau_0^{-1} \exp(-U_{eff}/kT) \quad (2)$$

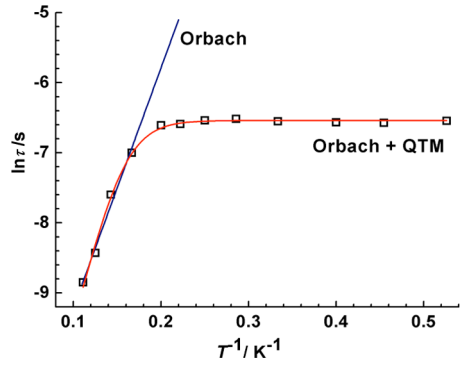

Figure 7. Magnetization relaxation time, ln τ, versus T^{-1} for **2** under a 1000 Oe dc field. The blue and red lines correspond to the best fit to the Arrhenius law and the best fit to an Orbach and QTM process.

where the thermally activated relaxation and QTM processes are both taken into account, affords the parameters U_{eff} = 50.2 K, $\tau_0 = 5.58 \times 10^{-7}$ s, and τ_{QT} = 0.00144 s. As expected, the value of the energy barrier, U_{eff}, is slightly higher than that obtained from the Arrhenius law when the effect of the QTM pathway is simultaneously considered. Furthermore, quasi-micircle shapes in the Cole−Cole plots in the temperature range of 1.9−9.0 K were obtained and were fitted to a generalized Debye model, yielding high values of α = 0.21−0.48 (Figure S11, Supporting Information) and implying a wide distribution of relaxation times.

In **3** and **4**, the χ'' component of the ac susceptibility (Figure 8, top, and Figure 9) merely shows a strong frequency dependence without peaks below 10 K under a zero dc field, which is suggestive of the onset of slow relaxation of the magnetization and the presence of possible fast QTM at low temperature, as observed in some polynuclear lanthanide systems.[45,46] Therefore, we could not accurately obtain the effective energy barrier by extracting the corresponding relaxation time owing to the lack of a maximum in the temperature window technically available. The case appears to be distinct from that in compounds **1** and **2**, which should arise from their distinct coordination environments with the changes in coordination anions, as revealed in the structural analysis.

Furthermore, we plotted $\ln(\chi''/\chi')$ versus $1/T$ over the frequency range of 30−1000 Hz (Figure S12, Supporting Information) and extracted estimated activation energies E_a of 2.1 K ($\tau_0 = 1.3 \times 10^{-4}$ s) and 1.2 K ($\tau_0 = 6.7 \times 10^{-5}$ s) for **3** and **4**, respectively, by applying linear fits based on the relation[47,48]

$$\ln(\chi''/\chi') = \ln(\omega\tau_0) + E_a/k_B T \quad (3)$$

To suppress the possible fast QTM, an optimal dc field was determined by measuring field-dependent ac signals (Figures S13 and S14, Supporting Information) for **3** and **4**. Never-

DOI: 10.1021/acs.inorgchem.5b00702
Inorg. Chem. 2015, 54, 5571−5578

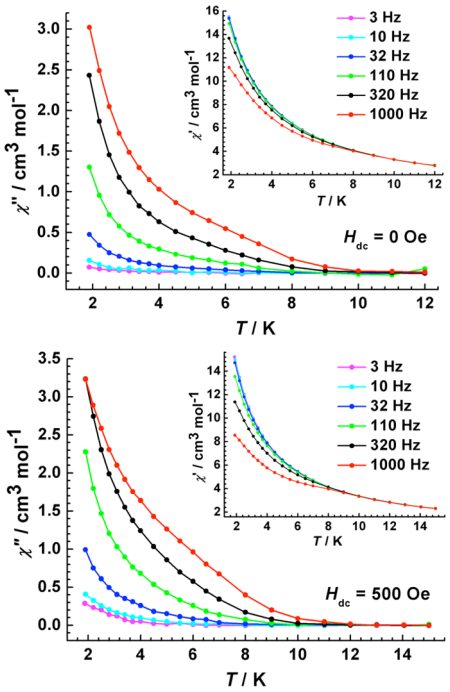

Figure 8. Temperature dependence of the out-of-phase ac susceptibility under dc fields of (top) 0 and (bottom) 500 Oe for **3**. Inset: Corresponding temperature dependence of the in-phase ac susceptibility.

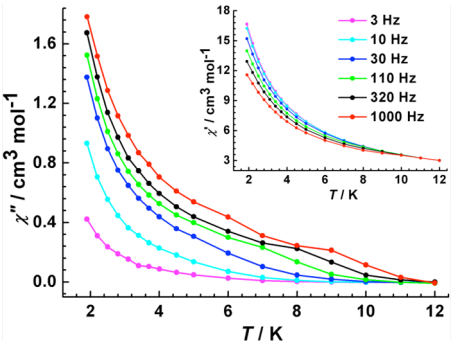

Figure 9. Temperature dependence of the out-of-phase ac susceptibility under zero dc field for **4**. Inset: Corresponding temperature dependence of the in-phase ac susceptibility.

theless, the application of an external dc field H = 500 Oe gave rise to negligible change in the temperature-dependent signals of the ac susceptibility for **3** (Figure 8, bottom), indicating that a QTM process under zero field is not an efficient pathway above 1.9 K.[15,49] Strikingly, strong frequency-dependent peaks of the out-of-phase ac susceptibilities were observed for **4** in the range of 1.9−10 K under a dc field of 900 Oe (Figure 10), as a clear indication that the application of a small static field makes a significant contribution to the effective suppression of QTM relaxation. Nevertheless, the relaxation time (τ) could not be clearly extracted from $\chi''(\nu)$ plots between 1.9 and 5.0 K on account of the intricate multiple relaxation process derived from the extremely distinct coordinated spheres of three Dy^{III} ions as a result of the coordination of the bulky terminal perchlorate ion in **4.** Above 6.0 K, only one thermally activated relaxation process existed, for which an Arrhenius fit (Figure S15, Supporting Information) of the data determined an

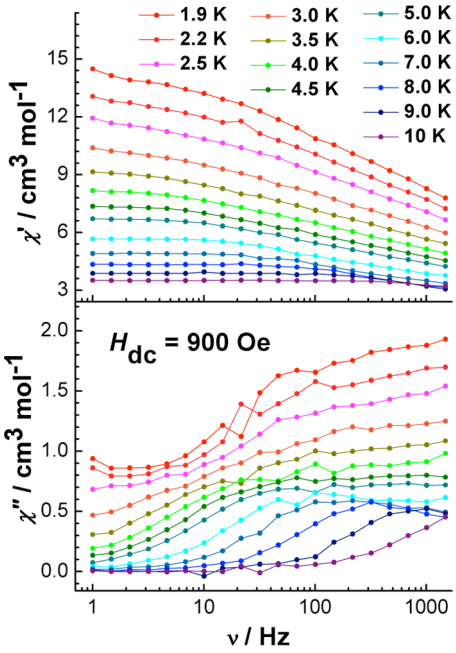

Figure 10. Frequency-dependent (top) in-phase and (bottom) out-of phase components of ac susceptibility under a 900 Oe dc field for **4**.

effective barrier of 34.5 K with a pre-exponential factor of 4.66 × 10^{-6} s.

CONCLUSIONS

A family of rare μ-$O_{acylhydrazone}$-bridged Dy_3 triangular circular helicates were successfully isolated using a new multidentate hydrazone ligand and various dysprosium salts. Remarkably, although all four compounds **1**−**4** exhibit similar static magnetic behaviors, the dynamic magnetic behaviors revealed by alternating-current (ac) susceptibility are quite distinct. Such dissimilar behaviors should be the result of the different terminal coordination solvent/anions around Dy3, being H_2O, Cl^-, NO_3^-, and ClO_4^- for **1**−**4**, respectively. The different sizes of the terminal ligands (H_2O, Cl^-, NO_3^-, and ClO_4^- for **1**−**4**, respectively) around the Dy3 ions give rise to significant differences in their local environments. For **1** and **2**, the close CShM values of all the three Dy^{III} ions are responsible for the similar multiple relaxation processes observed under zero dc field, and these magnetic behaviors can be assigned to the presence of different crystallographically independent Dy^{III} ions. However, the dramatic changes in the CShM values around Dy ions for **3** and **4** result in distinct dynamic magnetic behaviors with only a frequency-dependent out-of-phase signal without peaks under zero dc field. Such slight structural differences mentioned above probably affect the local tensor of anisotropy or the directions of the easy axes on each dysprosium site through the ligand fields of the terminal solvent or anions.[22,25] These results demonstrate that the size of terminal ligands (H_2O, Cl^-, NO_3^-, and ClO_4^- for **1**−**4**, respectively) around the Dy3 sites associated with subtle differences in their local environments have a direct and prominent influence on the dynamics of magnetic relaxation, which might offer a promising entry into the fine-tuning of the magnetic properties of SMMs by slightly adjusting the coordination geometry through variations in the size of the terminal ligands (solvent or anion).

DOI: 10.1021/acs.inorgchem.5b00702
Inorg. Chem. 2015, 54, 5571−5578

■ ASSOCIATED CONTENT

Supporting Information

IR spectra (Figure S1), crystal structures (Figures S2−S4 and Scheme S1), magnetic measurements (Figures S5−S15), and selected bond lengths and angles (Table S1). The Supporting Information is available free of charge on the ACS Publications website at DOI: 10.1021/acs.inorgchem.5b00702. CCDC-1056402 (**1**), 1056403 (**2**), 1056404 (**3**), and 1056405 (**4**) contain supplementary crystallographic data for this article. These data can be obtained free of charge from the Cambridge Crystallographic Data Centre via www.ccdc.cam.ac.uk/data_request/cif.

■ AUTHOR INFORMATION

Corresponding Author

*E-mail: tang@ciac.ac.cn.

Notes

The authors declare no competing financial interest.

■ ACKNOWLEDGMENTS

We thank the National Natural Science Foundation of China (Grants 21371166, 21331003, and 21221061) for financial support.

■ REFERENCES

(1) Sessoli, R.; Gatteschi, D.; Caneschi, A.; Novak, M. A. *Nature* **1993**, *365*, 141−143.
(2) Tang, J.; Hewitt, I.; Madhu, N. T.; Chastanet, G.; Wernsdorfer, W.; Anson, C. E.; Benelli, C.; Sessoli, R.; Powell, A. K. *Angew. Chem., Int. Ed.* **2006**, *45*, 1729−1733.
(3) Rinehart, J. D.; Fang, M.; Evans, W. J.; Long, J. R. *J. Am. Chem. Soc.* **2011**, *133*, 14236−14239.
(4) Zhang, P.; Guo, Y.-N.; Tang, J. *Coord. Chem. Rev.* **2013**, *257*, 1728−1763.
(5) Ungur, L.; Lin, S.-Y.; Tang, J.; Chibotaru, L. F. *Chem. Soc. Rev.* **2014**, *43*, 6894−6905.
(6) Dei, A.; Gatteschi, D. *Angew. Chem., Int. Ed.* **2011**, *50*, 11852−11858.
(7) Christou, G.; Gatteschi, D.; Hendrickson, D. N.; Sessoli, R. *MRS Bull.* **2000**, *25*, 66−71.
(8) Zhang, P.; Zhang, L.; Wang, C.; Xue, S.; Lin, S.-Y.; Tang, J. *J. Am. Chem. Soc.* **2014**, *136*, 4484−4487.
(9) Guo, Y.-N.; Xu, G.-F.; Gamez, P.; Zhao, L.; Lin, S.-Y.; Deng, R.; Tang, J.; Zhang, H.-J. *J. Am. Chem. Soc.* **2010**, *132*, 8538−8539.
(10) Ishikawa, N.; Sugita, M.; Ishikawa, T.; Koshihara, S.-y.; Kaizu, Y. *J. Am. Chem. Soc.* **2003**, *125*, 8694−8695.
(11) Benelli, C.; Gatteschi, D. *Chem. Rev.* **2002**, *102*, 2369−2388.
(12) Rinehart, J. D.; Long, J. R. *Chem. Sci.* **2011**, *2*, 2078−2085.
(13) Woodruff, D. N.; Winpenny, R. E. P.; Layfield, R. A. *Chem. Rev.* **2013**, *113*, 5110−5148.
(14) Guo, Y.-N.; Ungur, L.; Granroth, G. E.; Powell, A. K.; Wu, C.; Nagler, S. E.; Tang, J.; Chibotaru, L. F.; Cui, D. *Sci. Rep.* **2014**, *4*, 5471.
(15) Hewitt, I. J.; Tang, J.; Madhu, N. T.; Anson, C. E.; Lan, Y.; Luzon, J.; Etienne, M.; Sessoli, R.; Powell, A. K. *Angew. Chem., Int. Ed.* **2010**, *49*, 6352−6356.
(16) Rinehart, J. D.; Fang, M.; Evans, W. J.; Long, J. R. *Nat. Chem.* **2011**, *3*, 538−542.
(17) Blagg, R. J.; Muryn, C. A.; McInnes, E. J. L.; Tuna, F.; Winpenny, R. E. P. *Angew. Chem., Int. Ed.* **2011**, *50*, 6530−6533.
(18) Blagg, R. J.; Ungur, L.; Tuna, F.; Speak, J.; Comar, P.; Collison, D.; Wernsdorfer, W.; McInnes, E. J. L.; Chibotaru, L. F.; Winpenny, R. E. P. *Nat. Chem.* **2013**, *5*, 673−678.
(19) Pointillart, F.; Bernot, K.; Golhen, S.; Le Guennic, B.; Guizouarn, T.; Ouahab, L.; Cador, O. *Angew. Chem., Int. Ed.* **2015**, *54*, 1504−1507.
(20) Zhang, P.; Zhang, L.; Lin, S.-Y.; Xue, S.; Tang, J. *Inorg. Chem.* **2013**, *52*, 4587−4592.
(21) Bi, Y.; Guo, Y.-N.; Zhao, L.; Guo, Y.; Lin, S.-Y.; Jiang, S.-D.; Tang, J.; Wang, B.-W.; Gao, S. *Chem.—Eur. J.* **2011**, *17*, 12476−12481.
(22) Ungur, L.; Le Roy, J. J.; Korobkov, I.; Murugesu, M.; Chibotaru, L. F. *Angew. Chem., Int. Ed.* **2014**, *53*, 4413−4417.
(23) Zhu, J.; Wang, C.; Luan, F.; Liu, T.; Yan, P.; Li, G. *Inorg. Chem.* **2014**, *53*, 8895−8901.
(24) Liu, J.-L.; Chen, Y.-C.; Zheng, Y.-Z.; Lin, W.-Q.; Ungur, L.; Wernsdorfer, W.; Chibotaru, L. F.; Tong, M.-L. *Chem. Sci.* **2013**, *4*, 3310−3316.
(25) Habib, F.; Brunet, G.; Vieru, V.; Korobkov, I.; Chibotaru, L. F.; Murugesu, M. *J. Am. Chem. Soc.* **2013**, *135*, 13242−13245.
(26) Joarder, B.; Mukherjee, S.; Xue, S.; Tang, J.; Ghosh, S. K. *Inorg. Chem.* **2014**, *53*, 7554−7560.
(27) Chen, G.-J.; Guo, Y.-N.; Tian, J.-L.; Tang, J.; Gu, W.; Liu, X.; Yan, S.-P.; Cheng, P.; Liao, D.-Z. *Chem.—Eur. J.* **2012**, *18*, 2484−2487.
(28) Cucinotta, G.; Perfetti, M.; Luzon, J.; Etienne, M.; Car, P.-E.; Caneschi, A.; Calvez, G.; Bernot, K.; Sessoli, R. *Angew. Chem., Int. Ed.* **2012**, *51*, 1606−1610.
(29) Bain, G. A.; Berry, J. F. *J. Chem. Educ.* **2008**, *85*, 532−536.
(30) Tian, H.; Guo, Y.-N.; Zhao, L.; Tang, J.; Liu, Z. *Inorg. Chem.* **2011**, *50*, 8688−8690.
(31) Sheldrick, G. M. *SHELXS-97, Program for Crystal Structure Solution*; University of Göttingen: Göttingen, Germany, 1997.
(32) Guo, Y.-N.; Chen, X.-H.; Xue, S.; Tang, J. *Inorg. Chem.* **2011**, *50*, 9705−9713.
(33) Guo, Y.-N.; Xu, G.-F.; Wernsdorfer, W.; Ungur, L.; Guo, Y.; Tang, J.; Zhang, H.-J.; Chibotaru, L. F.; Powell, A. K. *J. Am. Chem. Soc.* **2011**, *133*, 11948−11951.
(34) Lin, P.-H.; Burchell, T. J.; Clérac, R.; Murugesu, M. *Angew. Chem., Int. Ed.* **2008**, *47*, 8848−8851.
(35) Anwar, M. U.; Dawe, L. N.; Tandon, S. S.; Bunge, S. D.; Thompson, L. K. *Dalton Trans.* **2013**, *42*, 7781−7794.
(36) Zou, L.; Zhao, L.; Chen, P.; Guo, Y.-N.; Guo, Y.; Li, Y.-H.; Tang, J. *Dalton Trans.* **2012**, *41*, 2966−2971.
(37) Novitchi, G.; Pilet, G.; Ungur, L.; Moshchalkov, V. V.; Wernsdorfer, W.; Chibotaru, L. F.; Luneau, D.; Powell, A. K. *Chem. Sci.* **2012**, *3*, 1169−1176.
(38) Wang, Y.-X.; Shi, W.; Li, H.; Song, Y.; Fang, L.; Lan, Y.; Powell, A. K.; Wernsdorfer, W.; Ungur, L.; Chibotaru, L. F.; Shen, M.; Cheng, P. *Chem. Sci.* **2012**, *3*, 3366−3370.
(39) Xue, S.; Chen, X.-H.; Zhao, L.; Guo, Y.-N.; Tang, J. *Inorg. Chem.* **2012**, *51*, 13264−13270.
(40) Lin, S.-Y.; Wernsdorfer, W.; Ungur, L.; Powell, A. K.; Guo, Y.-N.; Tang, J.; Zhao, L.; Chibotaru, L. F.; Zhang, H.-J. *Angew. Chem., Int. Ed.* **2012**, *51*, 12767−12771.
(41) Coxall, R. A.; Harris, S. G.; Henderson, D. K.; Parsons, S.; Tasker, P. A.; Winpenny, R. E. P. *J. Chem. Soc., Dalton Trans.* **2000**, 2349−2356.
(42) Ruiz-Martínez, A.; Casanova, D.; Alvarez, S. *Chem.—Eur. J.* **2008**, *14*, 1291−1303.
(43) Lin, P.-H.; Sun, W.-B.; Yu, M.-F.; Li, G.-M.; Yan, P.-F.; Murugesu, M. *Chem. Commun.* **2011**, *47*, 10993−10995.
(44) Guo, Y.-N.; Xu, G.-F.; Guo, Y.; Tang, J. *Dalton Trans.* **2011**, *40*, 9953−9963.
(45) Habib, F.; Long, J.; Lin, P.-H.; Korobkov, I.; Ungur, L.; Wernsdorfer, W.; Chibotaru, L. F.; Murugesu, M. *Chem. Sci.* **2012**, *3*, 2158−2164.
(46) Zhang, L.; Zhang, P.; Zhao, L.; Lin, S.-Y.; Xue, S.; Tang, J.; Liu, Z. *Eur. J. Inorg. Chem.* **2013**, 1351−1357.
(47) Bartolomé, J.; Filoti, G.; Kuncser, V.; Schinteie, G.; Mereacre, V.; Anson, C. E.; Powell, A. K.; Prodius, D.; Turta, C. *Phys. Rev. B* **2009**, *80*, 014430.
(48) Langley, S. K.; Moubaraki, B.; Murray, K. S. *Inorg. Chem.* **2012**, *51*, 3947−3949.
(49) Gamer, M. T.; Lan, Y.; Roesky, P. W.; Powell, A. K.; Clérac, R. *Inorg. Chem.* **2008**, *47*, 6581−6583.

DOI: 10.1021/acs.inorgchem.5b00702
Inorg. Chem. 2015, 54, 5571−5578